Available online at www.sciencedirect.com

ScienceDirect

Advances in Space Research 69 (2022) 1159–1169

ADVANCES IN SPACE RESEARCH (a COSPAR publication)

www.elsevier.com/locate/asr

Detection of radio interference in the UHF amateur radio band with the Serpens satellite

Gara Quintana-Diaz [a,*], Diego Nodar-López [b], Alberto González Muíño [b], Fernando Aguado Agelet [b], Chantal Cappelletti [c], Torbjörn Ekman [a]

[a] Department of Electronic Systems, Norwegian University of Science and Technology (NTNU), Trondheim 7030, Norway
[b] Escola de Enxeñaría de Telecomunicación, Universidade de Vigo, Vigo 36350, Spain
[c] Department of Mechanical, Materials and Manufacturing Engineering, University of Nottingham, University Park, Nottingham, UK

Received 11 March 2021; received in revised form 7 October 2021; accepted 9 October 2021
Available online 20 October 2021

Abstract

High packet losses when uplinking commands to small satellites have been reported in the UHF amateur band (430–440 MHz) since late 2013. Measurements of the uplink radio environment have shown high levels of in-band interference in previous works, but public measurement results are limited. Average interference levels are usually measured over some time to build heat maps. In this paper, the analysis is focused on sustained interference over a 24 ms time window using a maximum-minimum method. New heat maps and interference power distributions over Europe, Africa, the Middle East and the Americas were obtained using this method on measurements from the Serpens satellite. One of the missions of Serpens was to test an in orbit store-and-forward communication system to exchange short messages with ground sensors for disaster monitoring. The satellite operators had difficulties commanding the satellite due to interference, causing bit errors in uplink packets. Interference power of up to −70 dBm was detected during in-orbit measurements over Europe and North America, while expected received power from the ground stations was not more than −80 dBm. High power space-object tracking radars on the ground operating in the 420–450 MHz band could be the cause, but further measurements are required to verify this. Characterizing this interference can help develop mitigation techniques for future satellite communication systems.

Keywords: Interference measurements; UHF communication; CubeSats; Amateur radio

1. Introduction

Tracking, telemetry and control (TT&C) operations of small satellites have traditionally been performed in frequency bands below 1 GHz (von der Ohe, 2020). Most of these satellites have used VHF and UHF amateur radio bands with limited bandwidth (typically 25 kHz) (ITU-R: Report ITU-R SA.2312-0, 2014). Operators of this type of satellites experience difficulties when communicating with their satellites using the UHF band, especially when uplinking commands (Buscher, 2019; Busch et al., 2015). At Technische Universität Berlin (TU Berlin), loss of commands was experienced with the TUBSAT satellites over certain regions (Buscher, 2019). Uplink of commands to the UWE-3 satellite by the operators at Universität Würzburg was also challenging (Busch et al., 2015) due to interference in the 435–438 MHz band. In 2014, the average uplink failure rates for UWE-3 were 90–95% and reached 98–100% for some passes. Strong interference levels can prevent the correct demodulation of commands on the satellite receiver leading to limited satellite capabilities and loss of communication on some occasions.

* Corresponding author.
E-mail address: gara.quintana@ntnu.no (G. Quintana-Diaz).

https://doi.org/10.1016/j.asr.2021.10.017
0273-1177/

Similar problems were experienced during the Brazilian Serpens mission by the Universidade de Vigo (UVigo) team. The Serpens satellite had two missions: first, to serve as a technological demonstrator in the VHF band, and second, to test a UHF communication system as part of the Humanitarian Satellite constellation (HumSat) project. The latter offered a data store-and-forward system for ground sensor terminals (Aguado et al., 2012), enabling exchange of short messages with a packet-based machine-to-machine (M2M) communication system. The shorter revisit time of small satellites in low earth orbit (LEO) is useful for disaster monitoring efforts and data collection from ground sensors in remote areas (Santilli et al., 2018), both of which benefit from frequent observations to track environmental change over time.

Communicating with the Serpens satellite was challenging due to high packet loss rates on the uplink. In-orbit radio measurements were performed to investigate the cause of these difficulties. Strong interference signals affecting the uplink were detected over certain areas of the world. Short interference events can cause a high packet loss rate, even if the interference varies over time. Therefore, exploring the duration of the high-power interference signals is important for knowing the usable length of the communication packets. Analysing only average interference levels provides a superficial measure of the impact of the interference in a packet-based system. Strong and short interference bursts can have low average power but can cause enough packet error loss to prevent communication.

The focus of this paper is to estimate the severity of interference for satellites in LEO using the UHF amateur band 430–440 MHz and identify which geographical areas are affected by analyzing in-flight measurements from the Serpens satellite. The next section summarises the radio regulations in the frequency band and the state-of-art of radio frequency (RF) spectrum measurements in the UHF amateur radio band from space. In Section 3, the system architecture of the Serpens satellite and the measurement algorithm are described. The measurement results are presented in Section 4, followed by the discussion and a simple link budget in Section 5. Conclusions can be found in Section 6.

2. Related work

The frequency spectrum is a scarce resource for radiocommunication and its use is regulated by the International Telecommunication Union (ITU). Satellites use space radiocommunication services, and thus, the operators should send an advanced publication notice (API) to notify the ITU of the frequency assignment. If the satellite is part of the radio amateur service, the International Amateur Radio Union (IARU) should also be involved in the frequency coordination process for the amateur radio part of this band (ITU-R: Report ITU-R SA.2348-0, 2015).

Small satellites are not considered a separate class of satellites with regards to frequency filings, but they are referred to as *short-duration mission* satellites. The number of satellites with a mass between 1 and 10 kg launched during the past ten years has dramatically increased and is expected to keep increasing in the next years (ITU-R: Report ITU-R SA.2425, 2015). However, not all satellites have applied to the ITU for frequencies. Between 2003 and 2014, there were 341 nanosatellite and picosatellite launches, but only 31.4% had filed an API (ITU-R: Report ITU-R SA.2348-0, 2015). Therefore, knowing the real use of the frequency spectrum in space without measuring it is challenging.

The UHF spectrum is divided into many bands and each band is dedicated to one or more types of services depending on the ITU region (International Telecommunication Union, 2008). In the 430–440 MHz band, there are three services: amateur radio (430–440 MHz), radiolocation (420–450 MHz), and Earth exploration-satellite (432–438 MHz) (International Telecommunication Union, 2008). Amateur radio and radiolocation are primary services in ITU region 1; Earth Exploration-Satellite service is a secondary service. Secondary services may not create harmful interference to primary services and are not protected from interference generated by primary services. In ITU regions 2 and 3, amateur radio is a secondary service, while radiolocation is a primary service.

The radiolocation service includes high-power ground, airborne and shipborne radars. Some characteristics of the ground radars are described in the ITU-R M.1462–1 recommendation (ITU-R: Recommendation ITU-R M.1462-1, 2019). There are three types of ground radars: type A (space object tracking), type B (high altitude surveillance), and type C (surface and search). The characteristics of the radar types are summarized in Table 1. Type-A radars have transmit power of up to 5 MW and could cause interference in satellite uplinks since they are used for space-tracking. These radars operate all year round, scanning the sky from 3° to 60° of elevation and in 120° azimuth sectors. In Fig. 1, the locations of identified type-A radars according to ITU recommendations, are marked with red dots.

Due to the communication problems when uplinking commands to small satellites and the lack of knowledge of the real frequency usage and environment of the UHF band in space, a few universities and companies have started to measure the spectrum using satellites in the last few years (Aguado Agelet et al., 2015; Busch et al., 2015; Sarda et al., 2018; Buscher, 2019; Aurora Insight Inc., 2021). However, there is still a need for continuous spectrum monitoring because of the increase of small satellite launches, the fact that not all satellites file the required API to the ITU, and that public measurement data is limited. So far, the focus of most measurement studies has been to estimate heat maps and average interference values without considering the duration of strong interference or its power distribution.

Table 1
Characteristics of ground radars in the 420–450 MHz band (ITU-R: Recommendation ITU-R M.1462-1, 2019).

Parameters	Radar A	Radar B	Radar C
Peak output power (MW)	1–5	0.3	0.01
Antenna gain (dBi)	38.5	28–40	10
Polarisation	Circular	Circular	Circular
Pulse duration (ms)	0.25, 0.5, 1, 2, 4, 8, 16	0.01–16	0.001–1
Pulse frequency modulation	Search: 100–350 kHz chirp. Track: 1 or 5 MHz linear chirp	2 MHz linear chirp	1 or 0.3 MHz linear chirp
Pulse repetition frequency (Hz)	up to 41	15–400	100–3000
Antenna beamwidth in azimuth (°)	2.2	1.8 typical	80
Antenna beamwidth in elevation (°)	2.2	1.8 typical	60

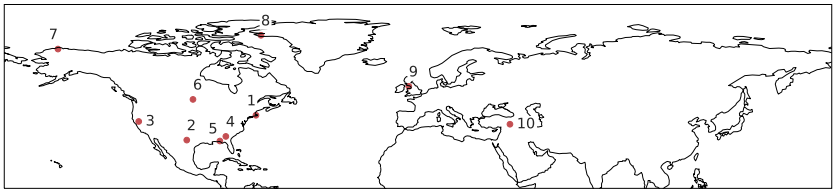

Fig. 1. Identified type A ground radar location in the 420–450 MHz band as defined in (ITU-R: Recommendation ITU-R M.1462-1, 2019; ITU-R: Recommendation ITU-R SA.1260-1, 2017). 1: Massachusetts (United States of America (USA)), 2: Texas (USA), 3: California (USA), 4: Georgia (USA), 5: Florida (USA), 6: North Dakota (USA), 7: Alaska (USA), 8: Thule (Greenland), 9: Fylingdales Moore (United Kingdom), 10: Pirinclik (Turkey).

The operators of the UWE-3 satellite at Universität Würzburg (Germany) experienced difficulties in the uplink in 2013–2014 and carried out in-orbit measurements in the 435–438 MHz band to investigate the problem. Using received signal strength indicator (RSSI) levels, the measured interference over central Europe was higher than over the Pacific. During a pass over Würzburg, the interference reached powers of −70 dBm at 437.385 MHz but was not detected at 436.6 MHz. The authors suggested that in-orbit reconfiguration of the carrier frequency could improve the link quality (Busch et al., 2015).

At UVigo (Spain) some preliminary measurements were performed after detecting strong interference in the test phase of the HumSat-D satellite in 2014. The communication system was based on the HUMsat PayLoad (HUMPL). Strong, pulsed interference was detected over the northern hemisphere in the 430–440 MHz band. The interference source was identified as one of the ground radars operating in the 420–450 MHz band from a site in the United Kingdom (UK) (Buscher, 2019). However, the measurements were limited to predefined frequencies and small areas, so the authors suggested the need to carry out further measurement campaigns and compare results with other satellites (Aguado Agelet et al., 2015).

There have also been two projects at TU Berlin (Germany) to monitor the frequency spectrum. In May 2018, a software-defined radio (SDR) payload was sent to the International Space Station (ISS) as part of the MarconiSSta project (von der Ohe, 2017). The goal was to measure received signals in space for the VHF, UHF, L-band, and S-band frequencies. The resulting heat maps made for the UHF band showed high average interference over both North America and Europe (Buscher, 2019). The payload was removed from the ISS in February 2019. As of the writing of this paper, the data is still being analysed. The use of an ISS-type orbit constrains the area of the sub-satellite points to between −51.6° and +51.6° latitude. In order to carry out measurements without this limitation, TU Berlin launched a small satellite called Spectrum AnaLysis SATellite (SALSAT) in September 2020 (Buscher, 2019).

Over the past six years, new businesses have emerged to address the increasing need for spectrum monitoring. Hawk Eye 360 (Sarda et al., 2018) and Aurora Insight (Aurora Insight Inc., 2021) are two companies that offer frequency spectrum data services by measuring the radio environment with their satellites. Hawk Eye 360 launched their second cluster of small satellites to geolocate RF emitters on the ground in January 2021, after demonstrating proof-of-concept with their first cluster (HawkEye 360, 2020). Aurora Insight has also begun commercial measurements of the frequency spectrum with small satellites. Their first satellite was launched in 2018 as an in-orbit demonstration mission and their second satellite was put into orbit in January 2021 (Aurora Insight Inc., 2021).

The contribution of this paper is to present a measurement methodology to detect strong sustained uplink interference and radio measurements from the Serpens satellite to complement existing measurement results. New heat maps and the power distribution of measured consistent uplink interference for areas in Europe, Africa, the Middle East and the Americas are estimated. Regions with low levels of consistent uplink interference are identified; these are better suited for M2M communication for collection of ground sensor data compared to regions with higher interference levels. Furthermore, this paper provides lessons learnt from these interference measurements that can be

used to tailor future measurement and analysis methods to improve interference characterisation.

3. Interference measurements with the Serpens satellite

The Serpens satellite was a Brazilian 3U Cubesat, launched on 17 September 2015 in an ISS-type orbit. The project was led by a consortium of Brazilian universities, with the participation of UVigo and several other international universities (Santilli et al., 2018). The satellite was divided into two different sectors for the different missions and payloads. Sector A was an educational project to demonstrate technology developed by a group of Brazilian universities. Sector B was developed by UVigo (Spain) and was part of the HumSat system. The HumSat project is an initiative from the United Nations Office for Outer Space Affairs (UNOOSA), the European Space Agency (ESA) and the International Astronautical Federation (IAF) to provide a communication system for remote areas or natural disaster areas. The idea is to provide the service by means of a constellation of small satellites with a store-and-forward communication system (Muíño and Agelet, 2014). In this paper, the focus is on the UHF communication mission in sector B.

Previously, the HumSat-D satellite was developed by UVigo as part of the HumSat project (Muíño and Agelet, 2014). In 2014, strong interference was detected in the uplink (Aguado Agelet et al., 2015). Lessons learnt from HumSat-D were applied on Serpens to enhance the mission. This included the implementation of an error-correction code in the radio protocol to mitigate the expected interference (Muíño and Agelet, 2014).

3.1. RF payload architecture

The communication payload in sector B (HUMPL) was used for in-orbit demonstration of communication between the satellite and ground terminals, and also for the interference measurements described in this paper. A turnstile antenna consisting of four monopoles was shared between TT&C and the payload.

The antenna interface in Fig. 2 consisted of the feeding network to adapt the signal to the monopoles and an antenna switch. The front-end of the payload was connected to the antenna switch to receive the RF signal. The front-end included a low noise amplifier (LNA) from Avago Technologies (MGA-62563), a passband filter from Golledge Electronics Ltd (TA0693A) and a splitter from Minicircuits (SCP-4-1+) as shown in Fig. 2. The splitter was connected to the receiver part of four transceivers from ON Semiconductor (AX5042) (Semiconductor Components Industries, LLC, 2016).

The center frequency and bandwidth of each receiver was configurable. For interference measurements, the payload used an operational mode with different configurations of bandwidth, centre frequency and measurement duration. COMMS mode was used for low-data rate M2M communication and simultaneous power measurements in the four receiver channels. The receiver channels had slightly overlapping bandwidths as seen in Fig. 3.

3.2. Interference measurement algorithm

The measurement algorithm used was designed for calculating the power of received packets which length was hundreds of milliseconds. This algorithm was implemented on the payload before launch. Due to uplink communication challenges experienced during satellite operations, the algorithm was configured, within its limitations, to measure the in-orbit interference environment. The configuration parameters used for the measurement analysis in this paper are summarized in Table 2. All the measurements presented in this paper were performed while the satellite's transmitter was switched off and were downlinked afterwards using limited data throughput. Power samples were obtained using the RSSI measurements in the AX5042 chips (Semiconductor Components Industries, LLC, 2016). The right length of the power measurement buffer (M) was calculated empirically during the development of the payload, analysing the error of the RSSI value estimated by the AX5043 transceiver in the laboratory. The value $M = 8$ was the minimum number of samples which yielded a reasonable error in the RSSI measure. These power samples were acquired from the received signal at the antenna port. Hence, the samples included the power of the interference and noise in space and the noise floor of the receiver. The power sampling frequency was

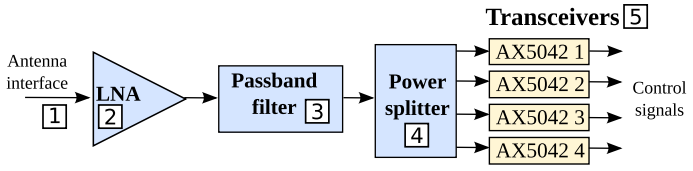

(a) RF payload architecture based on the diagram from (Muíño & Agelet, 2014).

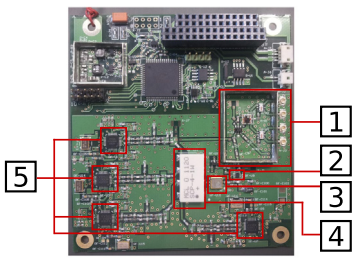

(b) Payload board adapted from UVigo (Aguado Agelet et al., 2015).

Fig. 2. HUMPL payload used both in HumSat-D satellite and Serpens satellite.

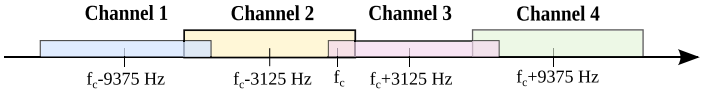

Fig. 3. Overlapping bandwidths of the four receivers in COMMS mode.

Table 2
Measurement parameters.

Parameter	Value
Measurement duration (s)	2–12
Bandwidth of receivers (kHz)	4 or 7.25
Bandwidth overlap (kHz)	1.25
Power sampling rate (samples/s)	333
Power sampling period (ms)	3
Length of power meas. buffer	8 samples (24 ms)

333 samples per second. The measurement duration could be configured.

The algorithm was based on a maximum-minimum approach applied to the power samples. Using the measurement duration and the power sampling rate, the total number of samples of the measurement (L) was calculated. The intention was to perform measurements as short as possible to try to determine the instantaneous power of each measurement, and two seconds was the minimum time the payload could be in reception mode. For this measurement duration, $L = 666$. Longer measurements were carried out for 12 s, $L = 4000$, as a comparison.

The power samples $P[n]$ were added to a circular buffer of length $M = 8$, vector $\bar{P}[n]$ with $n \in \{1, \ldots, L-(M-1)\}$. The algorithm estimated the maximum received power of sustained interference that lasted for at least the length of the buffer. The power samples $P[n]$ were added to the buffer as

$$\bar{P}[n] = [P[n] \quad P[n+1] \ldots \quad P[n+M-1]]^T \tag{1}$$

The first vector, for $n = 1$, was $\bar{P}[1] = [P[1] \quad P[2] \ldots \quad P[8]]^T$ and the next one was, $\bar{P}[2] = [P[2] \quad P[3] \ldots \quad P[9]]^T$. These column vectors can be seen as the result of applying a sliding window of length M to the power samples. These column vectors can form an $M \times (L/M)$ matrix like

$$\begin{aligned} \bar{\bar{P}} &= \left[\bar{P}[1] \quad \bar{P}[2] \quad \ldots \quad \bar{P}[L-(M-1)]\right] \\ &= \begin{bmatrix} P[1] & P[2] & \ldots & P[L-(M-1)] \\ P[2] & P[3] & \ldots & P[L-(M-1)+1] \\ P[3] & \ldots & \ldots & \ldots \\ \ldots & \ldots & \ldots & \ldots \\ P[M] & P[M+1] & \ldots & P[L] \end{bmatrix} \end{aligned} \tag{2}$$

The smallest entry (minimum) in each column formed the vector $\bar{P}_{min}$, where the k^{th} element was $\bar{P}_{min}[k] = min(\bar{P}[k])$. The output of the algorithm (P_D) was the largest (maximum) of all smallest power detected (minima), $P_D = max(\bar{P}_{min})$, during the measurement duration. This measurement method is an estimation focused on sustained interference levels to investigate how long the packets would be affected by strong interference. The output of the algorithm is the highest power sustained that lasts at least 24 ms and happens at least once in a measurement (in 2 or 12 s depending on the specific measurement duration). Therefore, the peak levels could have been higher for some occasions and for shorter periods of time.

4. In-orbit measurement results

Noise and interference measurements were carried out from October 2015 to March 2016. The heat maps in Fig. 4 show the interference for four 7.25 kHz sub-bands at different center frequencies in the 435–437 MHz band in October-December 2015. These measurements had a duration of 2 s. Sub-satellite points over Europe were strongly affected by the interference with levels up to −70 dBm, which were about 40 dB above the system noise floor.

Another series of measurements were taken at 435.391, 435.597, 435.803 and 437.809 MHz. Each measurement had a duration of 12 s. In Fig. 5, a global interference map of the 435 MHz frequencies shows higher levels of interference at the east and west coast of the United States. Since the interference must be higher than a given threshold for at least 24 ms to be stored by the measurement algorithm (Section 3.2), longer measurements rendered a higher probability of getting 24 ms segments with consistent high power. In Fig. 5, the areas that were the most affected by interference were the east and west coast of North America and central Europe.

In order to investigate how the interference power was distributed–and not just the common heat maps with average values–the empirical cumulative power distribution (ECDF) was calculated for different regions. Since the M2M communication system of Serpens was intended to work for South America, initial measurements were carried out in that area (green crosses in Fig. 6a). As a reference for a low interference distribution (also referred to as noise floor measurements in this paper) measurements over non-populated areas in the south Pacific and the south Atlantic were conducted (blue circles in Fig. 6a). There were four values of received power for each point which corresponded to the center frequency of the receive channels (437.516, 437.522, 437.528 and 437.534 MHz). The ECDF was estimated for both areas in Fig. 6. These measurements were taken with 4 kHz bandwidth, which was close to half the bandwidth of the other measurements in this paper (7.25 kHz). Hence, to compare both types of measurements, 3 dB was added to the power received in these cases. The received interference and noise were

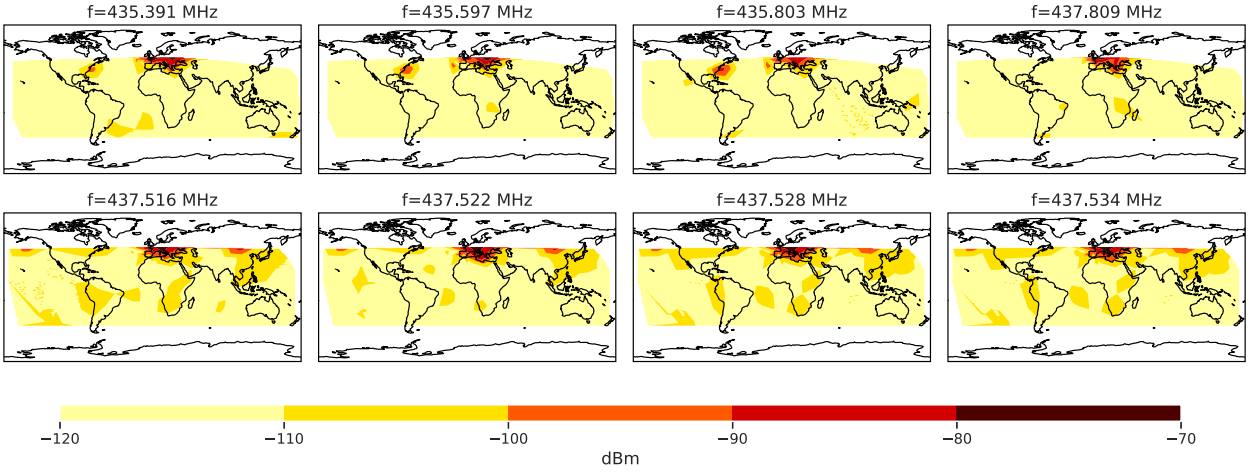

Fig. 4. Interference power measurement [dBm] world plot generated over several orbits (measurement duration of 2 s).

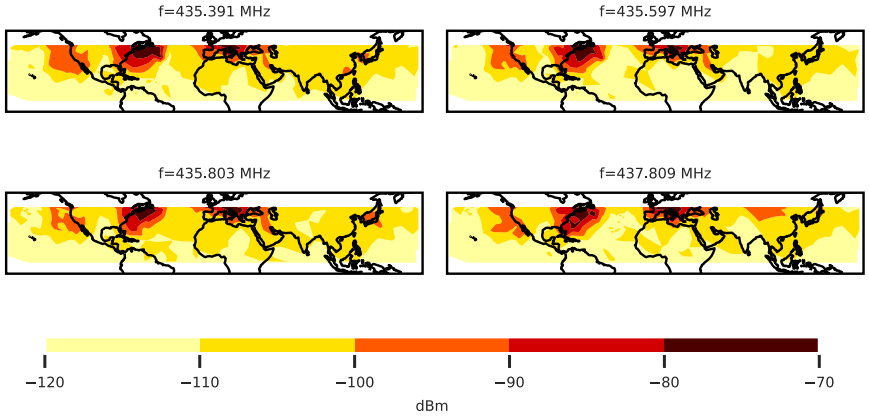

Fig. 5. Interference power measurement [dBm] plot generated over several orbits (measurement duration of 12 s).

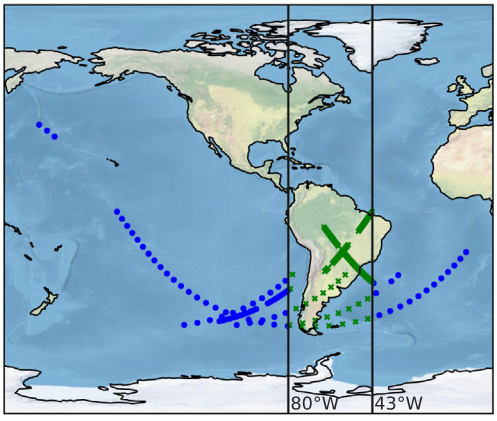

(a) Sub-satellite points for measurements over several orbits over the ocean (blue circles) and South America (green crosses). For each point there were four power values, one per frequency.

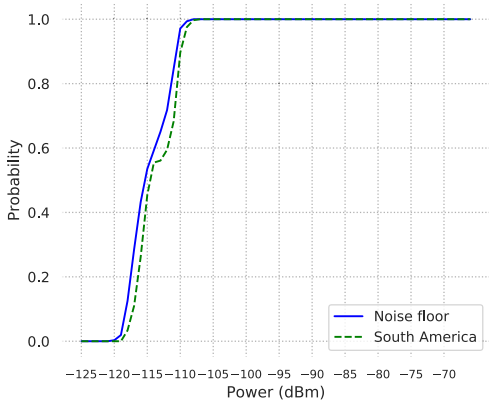

(b) ECDF of received power over the ocean (noise floor) and South America over several orbits. The ECDFs included four frequencies (437.516, 437.522, 437.528 and 437.534 MHz) since their power distributions were similar.

Fig. 6. Comparison of power distribution over the Pacific and south Atlantic ocean used as noise floor measurements, and areas of South America where ground sensor terminals could be located for M2M communication.

assumed to have a constant power density over the bandwidth. The power distribution over South America was similar to the one from the noise floor, but about 1 dB higher for 50% of the points. Two behaviours can be seen from the ECDF of the South American points: around 55% of the points experienced an interference power less than

−114 dBm, and the rest reached powers of about −107 dBm. Interference power over South America was low, with received power around 37 dB lower than the maximum interference power detected in the heat maps. Preliminary tests of the M2M communication system were performed in this area with adequate uplink performance.

The ECDF for the interference was estimated for four regions *R*1-*R*4 covering Europe, northern Africa and the Middle East (Fig. 7). In the map shown in Fig. 7a the northern parts of the plot were between 26.5° and 53° (marked with crosses in the map and with dashed lines in the plot) and southern parts were between 0° and 26.5° (circles in the map and continuous lines in the plot). Each region represented 35° of longitude. The points in the map represented the sub-satellite points where the satellite measured received power. There were four values of received power for each point, which corresponded to the center frequency of the receive channels (435.4, 435.6, 435.8 and 437.8 MHz). In Fig. 7b each line considered all the frequencies to estimate the ECDF. As a reference, the red curve was the distribution of all regions. There was a clear difference between the interference experienced in the regions in the north (*R*1 and *R*3) and south (*R*2 and *R*4). Regions *R*2 and *R*4 were affected in less than 20% of the points by signals with a power higher than −110 dBm. The power increased 15 dB in *R*3 and more than 22 dB in *R*1 for 20% of the points. In general, the sub-satellite points with a lower latitude experienced less interference because they were acquired over less populated areas and their distribution was closer to the noise measurement distribution (dotted black line).

In Fig. 8 the same procedure was applied to the measurements carried out over North America, redefining the areas of interest. Each region covered an area of 19° of latitude and 38° of longitude. The regions that were more affected by the interference were the northern regions (*R*5, *R*7 and *R*9). Around 27% of the points in region *R*5 and *R*7 experienced an interference level higher than −94 dBm and in region *R*9 higher than −78 dBm. Furthermore, in region *R*9 two different behaviours were observed: 75% of the points experienced interference levels above −109 dBm, while 25% of points did not. Satellites flying over this region will receive an interference power higher than −82 dBm for 50% of the time, reaching levels of −70 dBm on some occasions. In the southern regions *R*6, *R*8 and *R*10, where there were no known strong ground radars (Fig. 1), the power distributions were similar with a significantly lower mean as compared to the northern regions. These distributions were closer to the noise floor distribution (dotted black line).

The variation in interference power over the region was not due to measurements at different frequencies. In Fig. 8c and d a comparison between received power of two close carriers and two distant ones was plotted. The symbols for the regions were consistent with the ones used in Fig. 8a. The black dashed line showed the behaviour if the power in one carrier was completely dependent on the other and the red dashed lines, a difference of ±3 dB. In the left corner, the power of the carrier 435.4 MHz was plotted against the power in 435.6 MHz. It can be seen that when there was high power in one carrier, there was also high power in the other one. Hence, the interference seemed to have at least 200 kHz bandwidth. The difference in behaviour of the points in region *R*9 and *R*10 was highly visible. Most points in *R*9 were in the high interference area; the power in one frequency was strongly dependent on the power in the other frequency. In contrast, most points in *R*10 detected power at the noise level for both carriers. In Fig. 8d, the distribution of power was between a carrier at 435.4 MHz and another at 437.8 MHz. In this case, there were more points that were outside the ±3 dB region. This means that while high power was detected in one carrier, the other one did not detect as much because these points experienced narrow band interference. This interference may be caused by radio amateurs since the maximum bandwidth recommended for those services is 20 kHz.

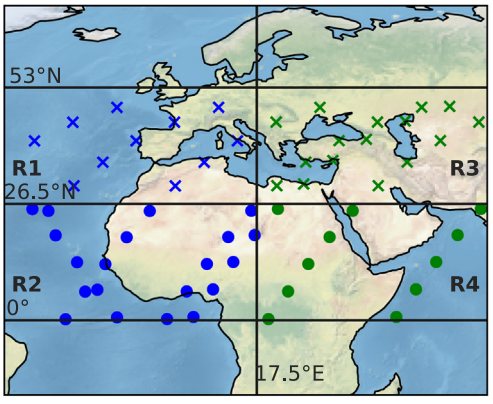

(a) Measurement locations over several orbits. Crosses were used for northern regions and circles for southern regions, blue for western and green for eastern areas. Each region covered 35° of longitude. Four frequencies were measured at each point (435.4, 435.6, 435.8 and 437.8 MHz).

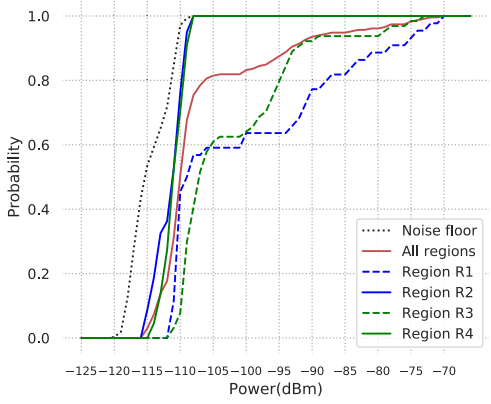

(b) ECDF of received power over the four regions and four frequencies, including the noise floor measurements (black dotted line). Continuous lines were linked to the circles in the map and dashed lines to crosses. Red line was the ECDF of all the points in the map.

Fig. 7. Power distribution over Europe, northern Africa and the Middle East (measurement duration of 12 s).

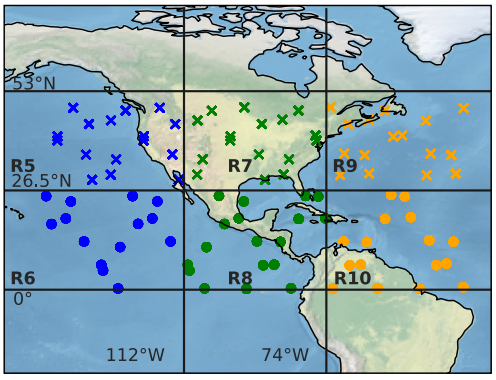

(a) Measurement locations over several orbits. Each region covered 38° of longitude. Four frequencies were measured at each point (435.4, 435.6, 435.8 and 437.8 MHz).

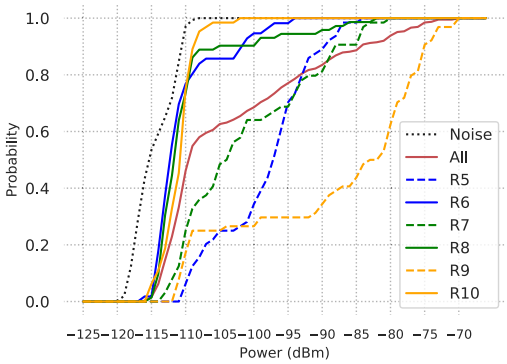

(b) ECDF of received power over the six regions and four frequencies, including the noise floor measurements (black dotted line). Continuous lines were linked to the circles in the map and dashed lines to crosses. Red line was the ECDF of all the points in the map.

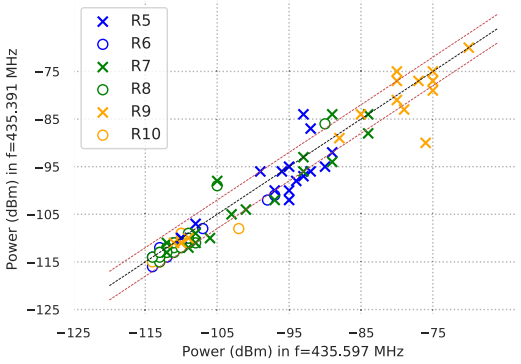

(c) Distribution of power over close carriers. The black dashed line showed the tendency if the power in one carrier was completely dependent on the other and the red dashed lines, a difference of ± 3 dB.

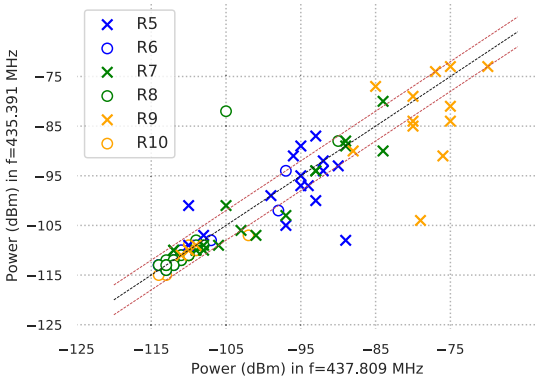

(d) Distribution of power over distant carriers. The black dashed line showed the tendency if the power in one carrier was completely dependent on the other and the red dashed lines, a difference of ± 3 dB.

Fig. 8. Power distribution over North America divided in six regions (measurement duration of 12 s). Crosses were used for northern regions and circles for southern regions, blue for western, green for central and orange for eastern areas.

The communication payload in Serpens was designed for M2M communication but was adapted to perform interference measurements. Despite the limitation in the measurement algorithm to determine signal time structure, there were some measurements that were compatible with the behaviour of radar sources. An example of a pass over the ground station in Vigo (Spain) suggested that a radar in the UK could be the cause of high interference. In Fig. 9a the power levels measured by the four receivers were mapped to the sub-satellite points where measurements were carried out, and plotted against the corresponding elevation towards the radar located in Fylingdales Moor. The measurements were 2 s long and the bandwidth of each receiver was 7.25 kHz. The PAVE PAWS radar in Cape Cod was used as a reference due to the public availability of specific information about its behaviour. The power levels measured follow the expected behaviour of a space-tracking ground radar changing from surveillance mode (lower elevation) to tracking mode (higher elevation), which is similar to the way the PAVE PAWS radar works (United States Air Force, 2009). When the satellite was above 10° elevation with respect to the radar, the measured power increased about 40 dB. The cross in the map was where the measured power experienced the first peak of interference. Furthermore, the measured power at the different frequencies was similar in this particular example. The separation between the centre frequencies of the receivers was around 18 kHz. If the interference was from a radar, it would be wide band (1–5 MHz for a type A radar in tracking mode), so all observed frequencies would be affected in a similar way.

Fig. 9b shows another example of a satellite pass over the same region with a different direction. In this case, the satellite was moving towards the south-east and the elevation of the pass with respect to the radar in the UK was below 10°, which means that the radar would not enter tracking mode. Still, an interference event can be seen 25 dB above the noise for a shorter period. This could be due to the radar operating in surveillance mode, where it searches for potential targets and switches between them.

The regions with high interference in the 430–440 MHz band were consistent with occurrences of type-A ground radars in Europe and North America (Fig. 1). However, there could also be other interference sources, such as ama-

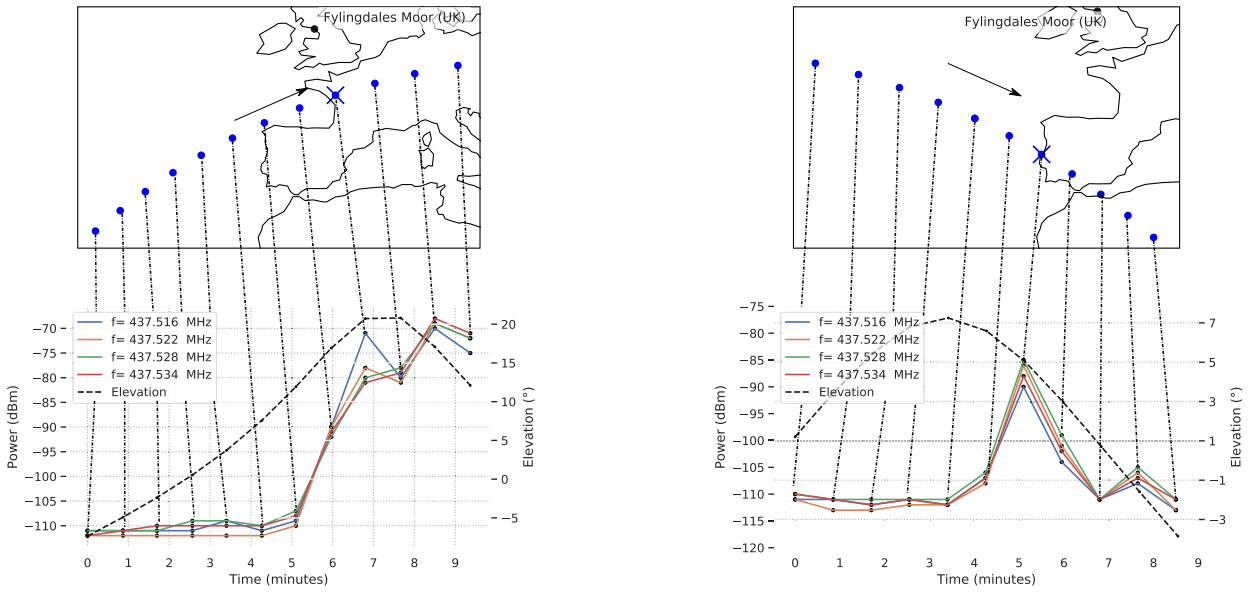

(a) North-east pass.

(b) South-east pass.

Fig. 9. Example of interference measurement of a pass over Vigo (Spain) at four different frequencies and with measurement duration of 2 s.

teur radio operators and communication with other satellites.

5. Discussion

Given the interference measurement results, an estimation of the uplink carrier to interference ratio (C/I) for a generic UHF ground station to a satellite can be done. The considerations are:

- Satellite orbit type: circular
- Satellite orbital height: 400 km.
- Carrier frequency: 437 MHz
- Ground station output power: 25 W (≈14 dBW)
- Ground station cable loss: 2 dB
- Circular polarised antenna.
- Antenna gain: 18 dBi.
- Minimum elevation of pass: 10°
- Maximum elevation of pass: 90°
- Propagation loss: free space and polarisation.

The effective isotropic radiated power (EIRP) is: $EIRP = 14 - 2 + 18 = 30$ dBW $= 60$ dBm. The free space loss is between approximately 137 dB (90° elevation) and 148 dB (10° elevation). Polarisation loss is 3 dB for a linearly polarised satellite antenna. The power received at the satellite is between −80 dBm and −91 dBm. If the interference power is −70 dBm, it would mean a (C/I) between −21 dB and −10 dB. It is very difficult for a communication system to cope with such a negative (C/I), as it leads to high packet loss in the uplink.

These (C/I) levels are not valid for average interference, but are instead valid for high sustained interference. The measurement method used enables the analysis of the probability that a sample will be over a certain power level for events 24 ms long in the 430–440 MHz band. The power levels measured over non-populated areas were considerably lower than in the rest of the world. Low interference power was detected over South America, making M2M communication for collection of sensor data from equipment on the ground possible. Over the higher latitudes in the European-African-Middle Eastern map, about 20% of the points were 16–24 dB above the noise floor and 18–35 dB for the higher latitudes of North American regions. Half of the points in the regions in Fig. 7a were 5 dB above the noise floor, and all points in Fig. 8a were 6 dB above the noise floor. This reflects how crowded the frequency spectrum is, based on real measurements, and gives an indication of why all the ground stations in Europe will experience difficulties when communicating with their satellites in the UHF-band. In North America, there was also a high level of interference in the higher latitudes shown in Fig. 8a. However, *R*9 is not a highly populated area and interference power was still 33 dB above the noise floor for 50% of the points. It can be an indication that the radar in Massachusetts (Fig. 1) makes a considerable contribution to the interference power such that ground stations in the area will experience an undesirable uplink quality. Due to the low interference levels detected over South America and the African regions, uplink communication performance will improve considerably if collaboration with ground stations in these areas is established.

Some lessons learnt from this study of interference can help plan future work. Planning the measurement campaigns based on which parameters will be calculated and the relevant areas of interest is extremely important. When repeating measurements over the different regions, the con-

figuration should be kept the same for a better comparison of results. Noise and interference measurements over non-populated areas are useful to establish the noise floor of the environment, including system noise. Building a hardware-in-the-loop setup that resembles the RF satellite architecture would make noise floor comparisons easier.

Future measurement missions to assess temporal properties of the interference environment could provide valuable information for the proper design of communication systems for small satellites operating in the 430–440 MHz band. Estimating the frequency and time structure of in-band interference from other small satellites in LEO is necessary to improve satellite communications. The results from this analysis can help other research groups to plan future measurements, since they have shown the areas with high consistent interference. The coasts of North America and central Europe, especially Vigo (Spain), are areas of interest for measurements since high interference has been detected. In addition, measurements above 51.6° and below −51.6° latitude should be pursued to get a global view and not be limited to the ISS orbit's constraints. In general, more measurement campaigns are needed to characterize interference thoroughly in both time and frequency to enable proper interference coping communication system design for this band. Spread spectrum techniques can protect from narrow band interference and interleavers can be useful for strong wide band interference. Error-correction algorithms, such as Reed-Solomon, are reliable for burst-noise channels (Consultative Committee for Space Data Systems: CCSDS 101.0-B-6, 2002).

6. Conclusions

In this paper, we presented a method to detect strong consistent uplink interference from satellites and used it in the Serpens satellite. We created new heat maps and interference power distributions plots in the 430–440 MHz amateur radio band over Europe, Africa, the Middle East, and the Americas. The results show that the regions over South America and specific areas over Africa have low uplink interference levels. Thus, data collection of ground sensor equipment for disaster monitoring over these regions is possible in the 430–440 MHz band.

The results also showed that there is strong interference affecting the uplink over Europe and the coasts of North America, reaching power levels of −70 dBm for at least 24 ms duration. Measurement results support and complement the findings in the works of TU Berlin (Buscher, 2019) and Universität Würzburg (Busch et al., 2015). The Serpens satellite measured at least 5 dB more power over populated areas than in non-populated areas in half of the measurements, reaching differences of up to 35 dB more power in 20% of the measurement points in some areas of North America. One possible source of interference may be the ground radars used for radiolocation in the band, since high interference was found in scarcely populated areas in regions with type-A radars. Interference counter-measures would not be needed in South America and Africa, thus, uplink communication to small satellites in the 430–440 MHz band can be achieved by establishing cooperation with ground stations in those areas.

In order to better understand the properties of UHF band uplink interference that a satellite can suffer in a LEO orbit in the UHF band, it is necessary to carry out more interference measurements with higher spatial, temporal and frequency resolution. Such measurements can be used to design an optimal communication system that can cope with interference events and increase the link quality.

Declaration of Competing Interest

The authors declare that they have no known competing financial interests or personal relationships that could have appeared to influence the work reported in this paper.

Acknowledgments

The authors thank the Brazilian Space Agency who financed the Serpens project and the Serpens consortium who managed the mission and the international cooperation. The work of UVigo is supported by Ministerio de Ciencia e Innovación in Spain (Grant No. ESP2016-79184-R). The work of Norwegian University of Science and Technology (NTNU) is supported by the Norwegian Research Council (Grant No. 270959), the Norwegian Space Agency, and the Centre of Autonomous Marine Operations and Systems (NTNU AMOS). Gara Quintana Díaz wishes to acknowledge the help of her colleague, Dr. Roger Birkeland.

References

Aguado, F., Tubío, R., Nodar, D., Castro, A., Vivas, E.V., Balogh, W., 2012. HUMSAT/ DEMO – The first CubeSat for the HUMSAT constellation. In: UN/Japan Nano-Satellite Symposium, pp. 1–5.

Aguado Agelet, F., Nodar López, D., González Muiño, A., 2015. Preliminary noise measurements campaign carried out by HUMSAT-D during 2014. In: ITU Conference and Workshop on the Small Satellite Regulation and Communication Systems. Prague, Czech Republic.

Aurora Insight Inc., 2021. Aurora Insight. https://aurorainsight.com/ (accessed: 2021-03-03).

Busch, P., Bangert, S., Dombrovski, S., Schilling, K., 2015. UWE-3, in-orbit performance and lessons learned of a modular and flexible satellite bus for future pico-satellites. Acta Astronaut. 117, 73–89. https://doi.org/10.1016/j.actaastro.2015.08.002.

Buscher, M., 2019. Investigations on the current and future use of radio frequency allocations for small satellite operations, vol. 7. Universitätsverlag der TU Berlin.

Consultative Committee for Space Data Systems: CCSDS 101.0-B-6, 2002. CCSDS recommendation for telemetry channel coding.

HawkEye 360, 2020. Rfgeo - hawkeye 360. https://www.he360.com/products/rfgeo/ (accessed: 2021-03-03).

International Telecommunication Union, 2008. Radio Regulations. ITU.

ITU-R: Recommendation ITU-R M.1462-1, 2019. Characteristics of and protection criteria for radars operating in the radiolocation service in the frequency range 420–450 MHz. Technical Report ITU.

ITU-R: Recommendation ITU-R SA.1260-1, 2017. Feasibility of sharing between active spaceborne sensors and other services in the range 420–470 MHz.

ITU-R: Report ITU-R SA.2312-0, 2014. Characteristics, definitions and spectrum requirements of nanosatellites and picosatellites, as well as systems composed of such satellites. Technical Report ITU.

ITU-R: Report ITU-R SA.2348-0, 2015. Current practice and procedures for notifying space networks currently applicable to nanosatellites and picosatellites. Technical Report ITU.

ITU-R: Report ITU-R SA.2425, 2015. Studies to accommodate requirements in the space operation service for non-geostationary satellites with short duration missions. Technical Report ITU.

Muíño, G., Agelet, A., 2014. Cubesat Constellations For Sensor Data Acquisition. In: IAA Cubesat Brasilia.

von der Ohe, M., 2017–2019. Marconissta. https://marconissta.com/ (accessed: 2021-03-03).

von der Ohe, M., 2020. Small satellite TT&C allocations below 1 GHz: outcome of ITU WRC-19. CEAS Space J. 12 (4), 565–571. https://doi.org/10.1007/s12567-020-00310-y.

Santilli, G., Vendittozzi, C., Cappelletti, C., Battistini, S., Gessini, P., 2018. CubeSat constellations for disaster management in remote areas. Acta Astronaut. 145, 11–17. https://doi.org/10.1016/j.actaastro.2017.12.050.

Sarda, K., Zee, R.E., CaJacob, D., Orr, N.G., 2018. Making the Invisible Visible: Precision RF-Emitter Geolocation from Space by the HawkEye 360 Pathfinder Mission. In: Proceedings of the 32nd Annual AIAA/USU Conference on Small Satellites. Logan UT, USA.

Semiconductor Components Industries, LLC, 2016. AND9354 - AX5042 Programming Manual. https://www.onsemi.com/pub/Collateral/AND9354-D.PDF.

United States Air Force, 2009. Pave Paws Early Warning Radar Operation Project Continued Operation of the Solid-State Phased-Array Radar System (SSPARS) also known as Pave Phased Array Warning Systems (PAWS) Cape Cod Air Force Station MA. Technical Report United States Air Force.